Rhythmic sampling of multiple decision alternatives in the human brain

Marcus Siems[1], Yinan Cao[1], Maryam Tohidi-Moghaddam[1], Tobias H. Donner[1], & Konstantinos Tsetsos[1,2]

[1] Department of Neurophysiology and Pathophysiology, University Medical Center Hamburg-Eppendorf, Hamburg, Germany

[2] School of Psychological Science, University of Bristol, Bristol, United Kingdom

Contact Information

Correspondence: m.siems@uke.de & k.tsetsos@bristol.ac.uk

Highlights

- Assessing covert attention in multi-alternative decision-making with magnetoencephalography (MEG)
- Rhythmic sampling as mechanism orchestrating attention between alternatives
- Focused information sampling alternates with attention switching between decision alternatives
- Covert attention allocation dissociates from oculomotor activity

Summary

During decision-making attention plays a pivotal role by guiding information sampling between alternatives. We need to optimally encode different options and compare between them. So far the role of attention in decision-making has only been addressed through saccadic displacements. However, looking is not always attending and attending not always looking. The influence of covert attention on decision-making is poorly understood. Here, we combined a three-alternative perceptual choice task with magnetoencephalography (MEG) recordings to chart covert attention during decision-formation. We found that rhythmic attentional sampling is a neurophysiological mechanism that can temporally disentangle the conflict between focusing and reorienting attention in decision-making. Embedded within an 11Hz oscillation focused processing and reorienting appeared at the peak and trough of the attention oscillation. Reorienting further intrinsically reset the oscillation and covert attention was dissociable from oculomotor activity. We thus propose that (covert) rhythmic sampling is a general cognitive mechanism harnessed to orchestrate flexible information processing in multi-alternative decisions.

Introduction

Imagine you're standing at a buffet trying to pick out a desert you'd like. To make an adequate decision between for example the apple pie and the tiramisu you will need to process each desert, i.e. the ingredients, appearance, personal preference, etc., and compare this information between options. In decisions requiring careful deliberation, attention plays a crucial as it orchestrates sampling information toward forming a decision[1–4]. Research bridging attention and decision-making has focused on where people look at and how this overt attention influences choices. For example, decision makers tend to look more and longer at options they will choose later[2,3,5] and gaze can further be influenced by the value of an option[1,6,7]. Fixating longer at one alternative makes one potentially overlook other features or alternatives creating thus a biased input to the decision-making process[8].

However, looking is not always attending[9–12] and the role of covert attention and information sampling for decision-making is poorly understood. For example while looking at the apple pie you might still compare it against your internal representation of the tiramisu. Little is known about the level of neural processing and which neurophysiological mechanisms might orchestrate switches across options or features during challenging decisions. In contrast to the recent literature that focused on where a decision maker looks at, here we address the more general and open question about how information is sampled and processed by the brain.

Particularly with perceptually noisy stimuli or challenging decisions there is a tradeoff between encoding and focusing on an option and the requirement to reorient attention between options to compare them[1,2,13]. Recent work on the neurophysiological basis of attention in simple perceptual tasks provides a potential mechanism that might resolve this conflict. Even during periods of sustained focus on a single stimulus, attention is not

static but oscillates[14–21]. This is evident in behavioral reports[15,16,18,22–28], and relates to neuronal activity in the theta[14,15,18,26,27,29], alpha[16,17,20,30,31] and gamma[23,24,26,29] frequency ranges.

One prominent idea is that the peak and the trough of the same cycle of the attention oscillation correspond to higher or lower depth of processing, i.e., attentional gain modulations[14,26]. When attention is at an oscillatory peak, processing of a selected stimulus is enhanced. Consequently, perceptual sensitivity to detect a target stimulus is larger during the peak of cyclic attention than during its trough[10,15,18,20,24,28,32,33]. By contrast, when at its trough, attention is relatively disengaged and can be shifted from one stimulus to another. Investigations in pupillometry and neuromodulatory systems further underline the distinction between an engaged and focused versus a disengaged and exploring attentional mode[34–40]. Rhythmicity thus appears to be a potentially universal mechanism that orchestrates information processing and routing by resolving competition between stimuli as well as processing stages, i.e. between sensory and motor systems[14,26,41–43].

During decision-making we would thus expect enhanced sampling of single alternatives during peaks and a higher tendency to reorient between options during troughs of the attentional oscillation. Here, we combined a three-alternative perceptual choice task with non-invasive magnetoencephalography (MEG) recordings that enabled us to chart the dynamics of covert spatial attention during decision-formation. Specifically, in decisions among multiple targets the value of each alternative needs to be encoded (requiring focused processing) and compared against the value of other alternatives (via reorienting attention). We leveraged this task to determine the neurophysiological mechanisms of attention allocation with millisecond precision and compare it against oculomotor activity.

As detailed below, we found evidence that the conflict between gathering additional evidence about a focused decision alternative and the tendency to reorient and explore other options is temporally resolved through rhythmic sampling. Embedded within an 11 Hz oscillations we found that 1) focused processing and reorienting occur at the peak and trough of the attention oscillation, 2) reorienting intrinsically resets the oscillation, and 3) these markers of covert attention are dissociable from activity of the oculomotor system. By showing how rhythmic sampling is harnessed to orchestrate flexible information processing in multi-alternative decisions, we propose that it is a general cognitive mechanism supporting behavior in tasks of increased complexity.

Results

We recorded non-invasive MEG from a total of 20 participants (9 female, age_{mean} = 28.05 years ± age_{STD} 4.6 years). The participants performed two interleaved tasks; a three-alternative perceptual decision-making task at threshold discriminability (decision-making task) and a flicker-detection task (sensory localizer; see Methods). Our experimental protocol for the decision-making task followed a three-alternative forced choice design with fixed response windows (Figure 1A). During central fixation three static Gabor-patches of varying contrast levels appeared in the periphery. We controlled for bottom-up sensory capture of attention by utilizing two different framing conditions that were randomly assigned at the single-trial level: Participants had to either choose the highest or the lowest contrast while the framing was only revealed after one second into the stimulus presentation. Because the framing decoupled the low-level features (i.e., contrast) from the task-relevance of the choice options, the task can probe goal-directed (top-down) allocation of attention and the results reported below are not affected by bottom-up sensory cortical responses. Participants performed the task at 77% accuracy (range = [66%, 86%]; Figure 1B) without any difference between the two task framings ($|t_{19}| < 1.7$; $p > 0.11$).

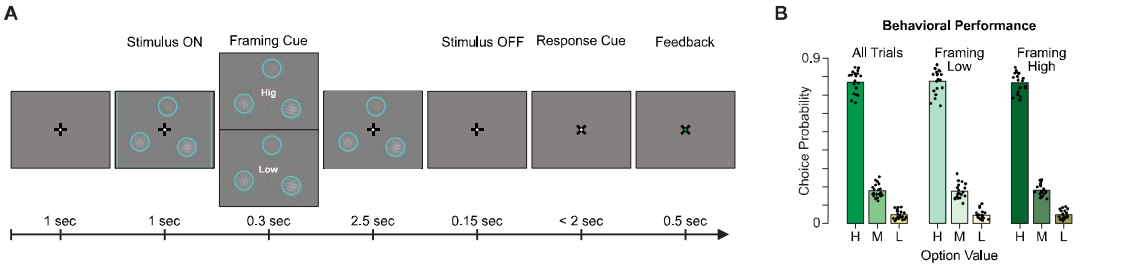

Figure 1. Experimental task & behavioral performance

(A) Trial structure of a three-alternative decision-making task with variable task framing. Stimulus size, contrast and eccentricity were changed for visualization purposes.

(B) Behavioral performance for all trials and within each framing condition. The dots indicate individual subject's performances.

We developed an approach to track the focus of covert attention during protracted decision processing. We trained an inverted encoding model[44,45] on the angular positions of stimuli during the sensory localizer to estimate the spatial focus of attention during the decision-making task (Figure 2A & S1). We followed the assumption that the neural representation, i.e. decodability, will be stronger for attended and weaker for unattended targets[13,22,29]. We further tracked the eye-gaze position to ensure central fixation and disentangle overt from covert attention allocation. Inverting the model yielded a time-resolved estimate of the response to each of the three angular positions during the decision-making task (Figure 2B). From the estimated responses we reconstructed the focus of spatial attention as the vector sum of the three channel responses (left, top, right). We focused on the resulting vector, referred to as ‘Attentional Vector’ in the following, to precisely track attentional fluctuations in the brain (Figure 2B). The vector length corresponded to the strength of attention and the angular similarity to the three stimulus positions corresponded to the locus of attention.

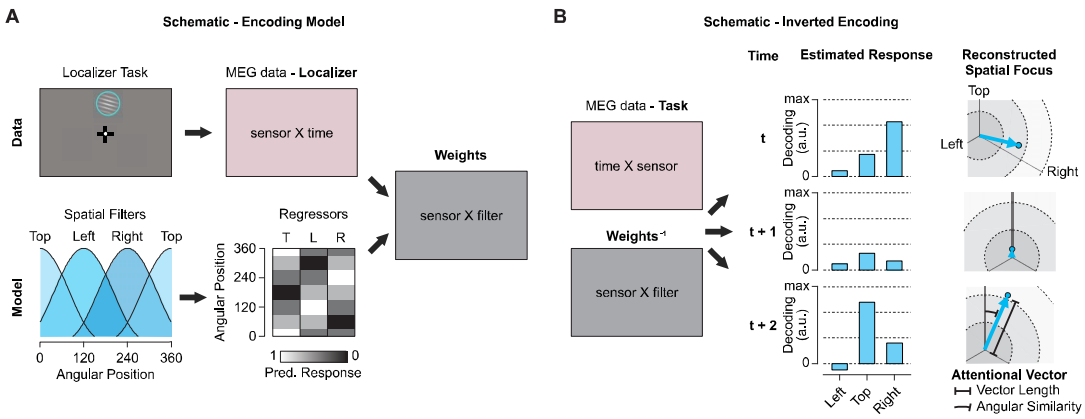

Figure 2. Reconstructing the focus of spatial attention with inverted encoding models

(A) Training the encoding model. The encoding model consists of a set of linear spatial filters defining the response given a certain stimulus. It comprises each information channels tuning curve, which discretized forms the Design Matrix. In combination with MEG data from the sensory localizer (see Methods) the weighting of the information channels within each MEG sensor can be estimated (GLM).

(B) Inverting the weights to estimate the channel responses during the decision-making task. We multiplied the inverted weighting matrix with the MEG data to estimate the response of the information channels at each time point. From the estimated responses we reconstructed the focus of spatial attention as the vector sum of the three spatial channel responses (left, top, right). The resulting Attentional Vector featured first, the length corresponding to the overall amount of attention and second, the angular similarity to the three stimulus targets.

Attention strength oscillates at around 11 Hz

We hypothesized that attention strength would vary throughout the course of the trial as a result of the trial structure. We hypothesized that goal-directed attention should be strongest early after the framing was revealed, i.e. after values have been assigned to the alternatives and a decision can be formed. In a first step we thus quantified the trial-averaged distribution of the vector length (Figure 3A). During the initial sensory interval, attention strength (i.e., vector length) steeply ramps up and displays three peaks; at around -0.8 s, 0.2 s and around 0.7-1.2 s from framing cue onset. We compared these results to the distribution of pupil diameter, a peripheral measure of task engagement[46–48]. Evoked pupil responses resembled, with more sluggish dynamics, the trial-averaged Attention Vector dynamics (Figure 3B; $r_{pupil,veclen} = 0.54$; $p < 0.05$).

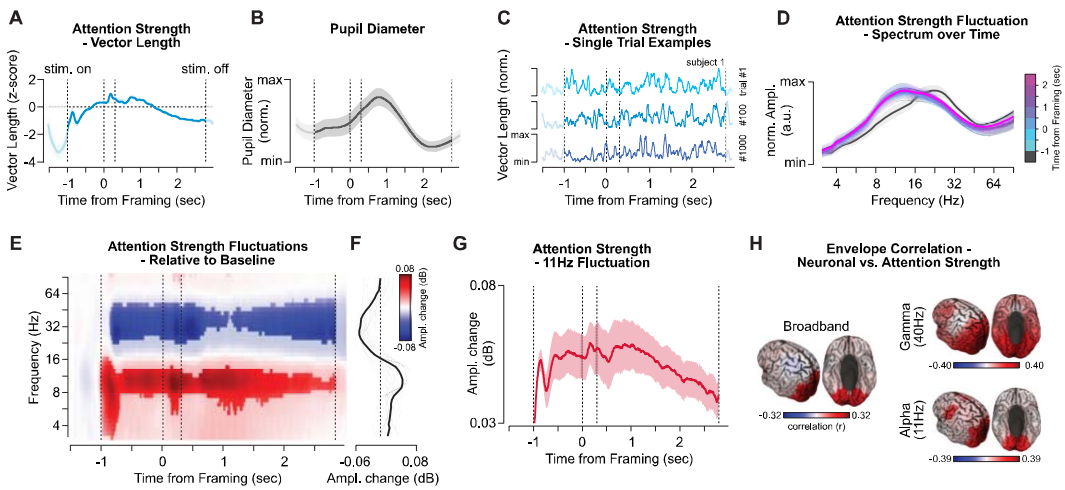

Figure 3. Attention strength fluctuates at around 11Hz.

(A) The distribution of the z-scored overall attention strength, i.e. vector length. The blue line indicates the average over trials and subjects. The shaded area indicates the standard error of the mean (SEM). Vertical dashed lines indicate the stimulus onset, framing cue onset and offset as well as the stimulus offset (from left to right).

(B) The average normalized pupil diameter during task execution. The thick line and shaded area indicate the average and the SEM over subjects.

(C) Single trial example traces of the normalized attention strength. The depicted trials are from subject 1, session 1.

(D) Windowed normalized amplitude spectra of attention strength fluctuations over the trial. Lines indicate the subject average, shaded areas display the SEM. The lines are color-coded according to the window onset (0.5 sec. window length) with regard to the framing cue.

(E-G) Frequency-specific change of attention strength amplitude relative to baseline. The frequency-wise amplitude strength values were normalized by dividing the average amplitude during the 0.5 seconds prior to stimulus onset and displayed in dB.

(E) Time-frequency resolved (TFR) distribution of the amplitude of attention strength fluctuations. Red and blue colors indicate an increase or decrease relative to baseline, respectively. The values were statistically masked at $p_{FDR} < 0.01$ within each frequency. Vertical dashed lines were defined as in (A).

(F) Average frequency-wise amplitude change, as in (E), throughout the stimulus ON period. Thick and thin lines display the average and single subject amplitude changes, respectively.

(G) Attention strength fluctuation amplitude at 11 Hz, relative to baseline in dB. Same data as in (C). Shaded area indicates the SEM.

(H) Correlation of the trial averaged amplitude envelopes between the neuronal signal (compare Figure S2) and the attention strength fluctuation. The correlation was computed for the broadband as well as frequency resolved signals. The values were statistically masked at $p_{FDR} < 0.05$ within each panel.

Importantly, there were substantial fluctuations of attention strength within each trial (Figure 3C), which we quantified with spectral analysis (Figure 3D-G). Attention strength fluctuated most strongly in the frequency range between 8 - 22 Hz (Figure 3D), with a clear increase from the pre-trial baseline (-1.5 to -1 seconds prior to framing) at 11 Hz, and decrease between 25 - 45 Hz (Figure 3E,F). The increase of the 11 Hz fluctuations was most pronounced between 0.5 seconds before until 1.5 seconds after the framing cue (Figure 3G).

Note that this increase in 11 Hz oscillations of attention strength is distinct from the commonly observed[49] suppression of cortical population dynamics we observed in the alpha frequency range and neighboring frequencies (Figure S2). Similarly, a broadband power decrease occurred for the raw decoding strength dynamics between 8 – 45 Hz (Figure S3). Thus, the increase in 11 Hz attention strength fluctuations emerges from the combination of information over the representations of different stimuli.

Along these lines, we further identified a direct relationship between attentional and neuronal dynamics for a large network including early and ventral stream visual- as well as lateral prefrontal areas (Figure 3H). Here, we correlated the time-frequency resolved time courses of the attention strength oscillations (compare Figure 3E) with the trial-averaged neuronal signal amplitude envelope (compare Figure S2) in the respective frequency ranges. Corresponding to the identified effects of attention strength modulation (Figure, 3G) we focused our analysis on the alpha (11 Hz) and gamma (40 Hz) frequencies as well as the broadband activity. This analysis yielded strong positive correlations of the attention strength with visual cortex activity ($r > 0.25$; $p_{FDR} < 0.05$; Figure 3H). Neuronal alpha-band and gamma-band envelopes further highlighted an

extended network of visual and prefrontal cortical areas (11 Hz & 40 Hz; $p_{FDR} < 0.05$; Figure 3H, right).

Moreover, frequency-specific attention strength fluctuations were correlated with task performance particularly for fluctuation frequencies between 8 – 16 Hz (Figure 4). We compared the attention strength between correct and error trials and found a qualitative trend for increased attention in the late decision-making phase of the trial for correct choices (Figure 4A; all $p > 0.2$). We further frequency-resolved this behavioral correlation (Figure 4B,C) and identified increased attention strength fluctuations related to choosing correctly from 1.5 seconds after framing until the end of the trial peaking in a frequency range from 8 – 16 Hz ($p_{FDR} < 0.05$). Importantly, we matched the included correct and error trials by difficulty and framing conditions (see Methods).

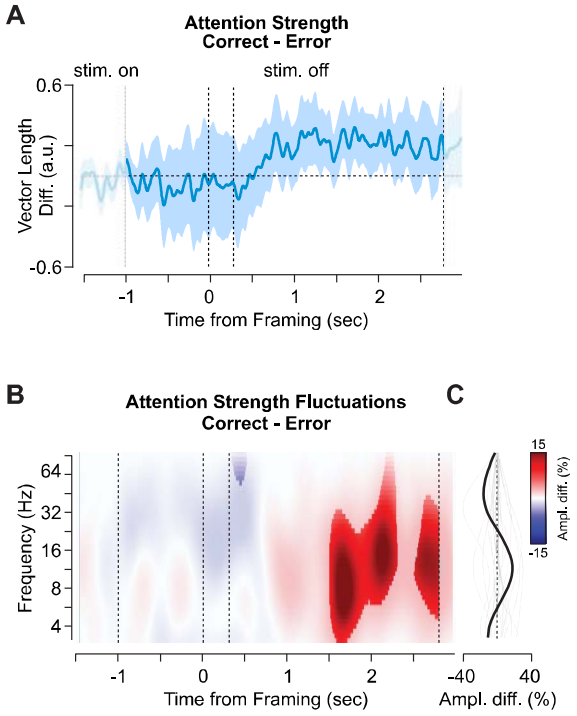

Figure 4. Attention strength fluctuations correlate with performance.

(A) The distribution of the overall attention strength difference, i.e. vector length, between correct and error trials (condition matched, see Methods). The blue line and shaded area indicate the average over subjects and the standard error of the mean (SEM). Vertical dashed lines denote the stimulus onset, framing cue onset and offset as well as the stimulus offset (from left to right).

(B-C) Time-frequency resolved (TFR) attention strength fluctuation differences between correct and error trials as percent change to correct.

(B) The distribution of TFR amplitude differences (correct-error) over the full spectrum and trial

duration. The values were was statistically masked at pFDR< 0.05 over the spectrum.

(C) Frequency-wise amplitude change, as in (B), averaged over the stimulus ON period. Thick and thin lines display the average and single subject amplitude changes, respectively.

Refocusing and switching of attention are nested within an 11Hz rhythm

The above analyses uncover clear modulations of attention in two frequency bands: an increase at around 11 Hz and a decrease around 40 Hz. Thus, our results display how information sampling at a focused decision alternative can oscillate. However, we do not know yet how attention is allocated between options and whether allocation samples options in a similarly rhythmic fashion? Theoretically, attention strength might fluctuate even without the locus of attention shifting to a new stimulus. Conversely, attention shifts (reorienting) between stimuli might not necessarily be coupled to changes in attention strength. Based on existing literature we hypothesize an increased tendency to reorient attention to a new stimulus when attention strength is weak[14,26]. We assessed this relationship directly.

We used the angular similarity to track the intrinsic dynamics of attention switching. At each point in time, we assessed angular similarity of all three options (top, left and right) to the orientation of the attentional vector. The maximum out of the three angular similarities describes the option that best matched the momentary attentional focus. This maximum will be high when one of the three options is in focus and low when attention is located between options. The maximum angular similarity (MAS) did not show systematic dynamics across the trial (Figure 5A), indicating that attentional reorienting could occur at any time point throughout the trial. Reorienting attention between stimuli has been conceptualized as rapid covert events – in other words 'attentional saccades'[10,16,50,51]. To track such events, we discretized attentional allocation into brief

events by thresholding the maximum angular similarity. MAS was defined in a circular space and thus even under completely random conditions or when decodability of the options cannot be granted it will still pass a threshold and we would infer attention to be allocated to one of the three options at random times. We thus included a second threshold on the vector length to exclude purely noise-driven events as much as possible (Figure 5B & S4). This approach enabled us to assess directly when attention stayed at the same option or switched to a different one.

We then quantified the lengths of the intervals between attentional events (inter-event-intervals, IEI; Figure 5C). For a random Poisson process (i.e., no temporal structure), the IEI histogram would display an exponential decay of probability with interval duration (Figure 5C,D, dashed lines; see Methods). We identified clear deviations from this prediction for the attention allocation, at short interval lengths up to 0.13 seconds and at around 0.18 seconds interval length ($p_{FDR} < 0.05$; Figure 5C). An increase at short latencies between events highlights a burst-like pattern of event occurrences. These results thus indicate clear temporal structure between events.

Further splitting attentional events by sequential structure revealed a nested profile of rhythmic sampling of choice (Figure 5D-G). We sorted attentional events into two types of first-order sequences of attention allocation: (i) staying at the same decision alternative, and (ii) switching to a new alternative. Indeed, staying and switching attention events exhibited distinct temporal structures: Staying peaked at interval lengths of around 0.1 s and 0.18 s; by contrast, switching followed the previous event after around 0.05 s and 0.15 s (Figure 5D,E).

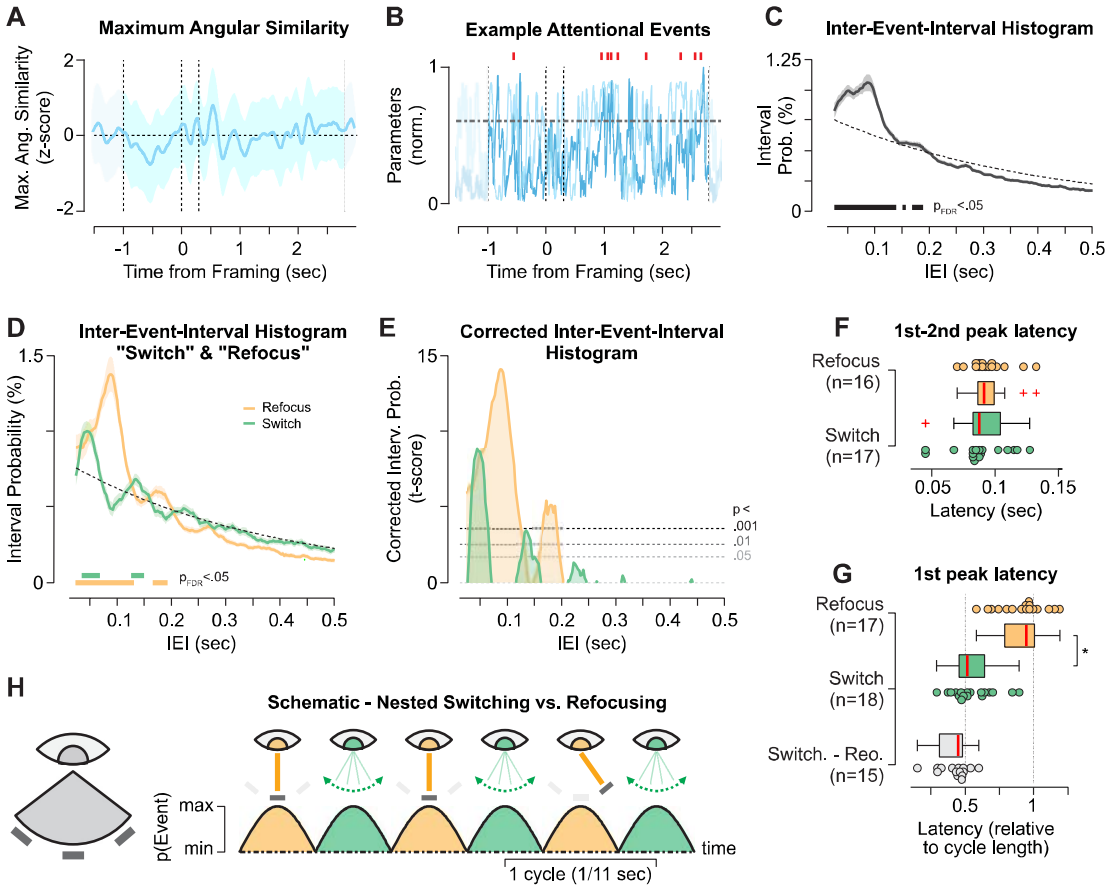

Figure 5. Attention allocation to distinct stimuli is nested within an 11Hz rhythm.

(A-B) Defining and describing covert attentional saccades using the attentional vector orientation.

(A) Maximum angular similarity to the three stimuli on screen, averaged over trials. The light blue line indicates the z-scored average over subjects. The shaded area displays the SEM. Vertical dashed lines indicate the stimulus onset, framing cue onset and offset as well as the stimulus offset (from left to right).

(B) Schematic definition of attentional saccades in an example trial. An attentional saccade (red mark) is defined as a moment in time when the vector orientation aligns with one of the three presented stimuli (thresholded at 90% percentile maximum angular similarity). Yet, also for random data the vector orientation will align due to its uniform distribution. Thus, we included a second threshold on the vector length (90% percentile), i.e. the overall attention strength.

(C) Inter-event-interval (IEI) histograms over all trials and attentional events. The data was normalized to the sum of all intervals displaying the interval probability. The black line indicates the average over subjects, the shaded area the SEM. The black bars denote significant ($p_{FDR} < 0.05$) interval probabilities exceeding the histogram for random events (dashed line, see Methods for details).

(D-G) Inter-event-interval properties separately for refocus (orange) and switch (green) attentional events. Refocus and Switch describe events that focus at the same or a different target location as the prior event, respectively.

(D) Inter-event-interval histograms separately for refocus (orange line, ± SEM) and switch (green line, ± SEM) attentional events. The bars denote significant ($p_{FDR} < 0.05$) interval probabilities exceeding random

events, color-coded as above.

(E) Same data as in (D) now displaying corrected IEI as t-score against random (dashed line in (E)). Horizontal dashed lines indicate the uncorrected significance-levels and zero.

(F) Box-plots of latencies between the first and second peak within the IEI histograms. Colored dots display single subject values, color-coded as above.

(G) First peak latency relative to the cycle length as described in (F). Asterisk denotes a significant difference between switch and refocus ($p_{FDR} < 0.05$). Vertical dashed lines display half and full cycle length offset. N denotes the number of subjects with identifiable (at least one (F) or two (G)) significant peaks within the IEI histogram.

(H) Schematic - Covert attention allocation , i.e. attentional saccades, were nested within the underlying 11 Hz rhythm. Here, two distinct sets of attentional events, either refocusing on the same stimulus or shifting the focus of attention to a different stimulus (Figure 4D-F). Both attentional event-types were further offset by about half a cycle within the 11 Hz rhythm (Figure 4G).

Both sequence types displayed rhythmicity in their temporal profiles: If we assume that events occurred at distinct phases of an underlying rhythm we would expect peaks of IEI probability in the first cycle, the second cycle, the third cycle, etc., of this oscillation. We encountered reappearing local maxima in the corrected interval histograms for both event types (Figure 4E & S5). We quantified the rhythmicity as the latency between the first and the second significant peak of the corrected histograms within each subject (Figure 5F). Both staying and switching events displayed approximately 0.09 s first-to-second peak latencies – in other words, rhythmicity at 11 Hz.

Critically, staying and switching were nested, at opposing phases, within the same 11 Hz oscillation (Figure 5G). We directly compared the temporal offset between staying and switching through their initial inter-event-interval maximum (Figure 5G-H). According to the individual attention cycle length (Figure 5F), we identified the first switching peak at around 0.5 (median = 0.51 cycle length, $range_{25\%-75\%}$ = 0.46 - 0.64) and the first refocusing peak at a full attention cycle length (median = 0.95 cycle length, $range_{25\%-75\%}$ = 0.79 - 1.01) from the previous event (Figure 5G). Even though the individual first peak latencies varied across participants, the phase-shift between switching and staying was

consistent (slightly below half a cycle; median = 0.45 cycle length, $range_{25\%-75\%}$ = 0.31 - 0.48; Figure 5G, grey box). Thus, staying events coincided with the peak, of the attention strength oscillation and switching occurred during the trough.

Note that, if attentional events would occur simply as a function of an oscillation in attention strength, we would expect double as many peaks within the interval probability histograms. That is, switching events would occur predominantly either a full or half a cycle after the previous event depending on whether this was a staying or switching event, respectively (Figure S6A). And vice versa for staying events. Yet, independent of the event history, the IEI probabilities within event types indicated the same temporal profiles (Figure S6B-C). In other words, the offset between switch and stay peak IEIs (Figure 5D-G) was not a trivial consequence of the rhythmic fluctuations of attentional strength identified in Figure 3. Instead, attentional events seemed to interact with the attention strength oscillation in a way that we illuminate further in the next section.

In sum, the results of this section indicate that switching was associated with attention disengagement and staying occurred within a focused attentional state – that is, refocusing attention on the previously sampled decision alternative (Figure 5H). Attentional events, therefore, provide a deep window into the dynamics of covert attentional sampling during decision formation.

The recent literature further highlighted pupil size as a peripheral measure related to reorienting attention[52–54]. As a control analysis we thus further computed the pupil size as well as the change in size, i.e. the temporal derivative, in relationship to attentional saccades (Figure S6). We identified a positive relationship of pupil diameter with the occurrence of refocusing events (r_{mean} = 0.10, p = 0.004; Figure S6C) as well as a larger

pupil diameter during refocusing ($p = 0.005$; Figure S6D). On the other hand, attentional switches were negatively correlated with the change in pupil size ($r_{mean} = -0.07$, $p = 0.01$; Figure S6C) and displayed event-triggered pupil constriction ($p = 0.01$; Figure S6D). Our findings thus do not hint towards increased pupil reaction during reorienting. Rather, pupillometric measures appear to display a link to general task engagement and information sampling[34–37,40].

Attentional events reset rhythmic attention strength fluctuations

Attentional events appear to not only follow but also reciprocally impact the attention strength fluctuation (Figure 5 & S7). We thus examined peri-event attention strength to unravel event-triggered changes in its dynamics. In a time-window from -0.2 prior to 0.2 s after each event we averaged attention strength over all refocusing and switching events separately (Figure 6A). Prior to an event, the traces of attention strength were largely unaligned (mean $r_{pre} = -0.10$, $r_{pre,25\%-75\%} = -0.22 - 0.42$; $p > 0.10$; correlations on detrended signals, compare Figure 6B). By contrast, after the event, the attention strength traces became strongly synchronized (mean $r_{post} = 0.99$, $r_{post,25\%-75\%} = 0.97 – 0.998$; $p < 10^{-23}$; correlations on detrended signals). Similarly, the fluctuations of the attention locus, i.e. the maximum angular similarity, displayed compatible event-triggered dynamics (Figure S8).

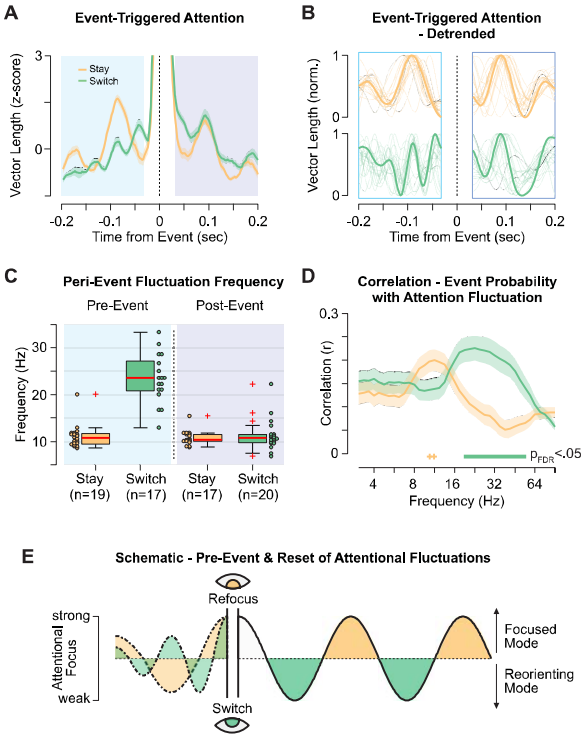

Figure 6. Peri-event fluctuations of attention strength.

(A) Attentional event-triggered average of the z-scored attention strength, i.e. vector length (see Methods). The colored lines and shaded area indicate the average and SEM over events and subjects separately for refocusing (orange) and switching events (green). Pre- and post-event epochs are highlighted in blue and purple.

(B) The same data as in (A) detrended individually pre- (-0.2 to -0.03 s) and post-event (0.03 to 0.2 s). The data was smoothed with a 0.025 s boxcar kernel for visualization.

(C) Dominant peri-event fluctuation frequencies defined via the average peak-to-peak latency within each epoch (B). N denotes the number of subjects for which a sine-fit was possible.

(D) Correlation between the attentional event probability (Figure S9) with the amplitude of the attentional fluctuations (Figure 3E) over the stimulus ON period. Lines depict the average, shaded areas the SEM over subjects. Thick lines below indicate significant differences between event types ($p_{FDR} < 0.05$) and crosses a statistical trend for significance ($p_{FDR} < 0.1$).

(E) Schematic - pre-event activity and reset of attentional fluctuations. Switch events occurred predominantly around the peak of a preceding a 22 Hz oscillation, faster than the attentional rhythm and activity preceding Refocus events (Figure 6C). However, Switch attentional saccades appeared to reset the ongoing attention fluctuation and synchronize post-event activity (Figure 6A-C).

Moreover, attention strength fluctuations also exhibited distinct frequency profiles before and after switching events, fluctuating at higher frequencies specifically before switches

(Figure 6A-B). We fitted a sine wave to both epochs, pre- and post-event, and for both event types separately to estimate their dominant frequency content. Attention strength fluctuated at around 11 Hz before and after refocusing events, as well as after switching events (Figure 6C). However, prior to switching, there was a prominent increase ($p < 10^{-6}$) of the fluctuation frequency to around 22 Hz. Switch events thus appear to reset the ongoing attention strength fluctuation to the attentional up-state, the focused mode.

The faster dynamics prior to switching the focus of attention further corresponded to the appearance of high-frequency modulations of attention strength throughout the trial. We correlated the attention fluctuation amplitude in each frequency range (compare Figure 3E) with the event probability over the course of the trial (Figure S9). Event probabilities were positively correlated with the attention fluctuation amplitudes over the entire spectrum (Figure 6D). However, a stronger 11Hz attention modulation predicted more refocusing events (Figure 6D, orange line) and a stronger modulation between 19 - 40 Hz more switching events (Figure 6D, green line). Neuronal activity correlations further supports this dissociation between switch and refocusing events in an extended visual and lateral prefrontal cortical network (Figure S10).

The results suggest that refocusing events are a discrete extension of the attention strength fluctuations: i.e., higher attention strength are associated with more refocusing events. On the other hand, switching events differed from refocusing in both, time and their dynamical properties. Attentional switches, embedded in down-phases of oscillating attention, thus offer an neurophysiological mechanism to disentangle the tradeoff between prolonged focusing on one decision alternative and the need to reorient attention between alternatives to compare them.

Dynamics of covert attention can be dissociated from fixational eye movements

Because overt and covert attention are linked[9,11,23,52,55–57], one might wonder whether and how the rhythmic fluctuations of covert attention we have identified above might relate to the dynamics of overt, fixational eye movements. In other words, does looking affect attention to different decision alternatives? Applying eye-tracking we assessed the microsaccade rate and identified pronounced variation with the trial structure (Figure 7A). Compatible with to the attentional event analysis we computed the inter-saccade-intervals (ISI) over the stimulus period. ISI displayed a single peak at around 0.25 s (Figure 7B).

Microsaccade rates were further increased prior to attentional switching but not refocusing. We computed the attentional event-triggered microsaccade rate and identified a prominent increase around 0.15 s explicitly before switching events (Figure, 7C; $p_{FDR} < 0.05$). Conversely, microsaccade-triggered attention strength was strongly increased post-saccade at around 0.17 s (Figure 7D). We further correlated the average MS rate over the trial with the corresponding attentional event probability within each subject (Figure 7E). Attention switches hereby positively correlated ($r = 0.06$; $p < 0.02$) with the MS-rate. Further, we found relatively more switch (mean = 35%, range = 25 – 50%) than refocus events (mean = 26%, range = 17 – 38%; $t_{19} = -13.2$, $p < 10^{-9}$) were preceded by microsaccades (Figure 7F). Thus, microsaccades appear to play a prominent role in the reorienting of attention between decision alternatives.

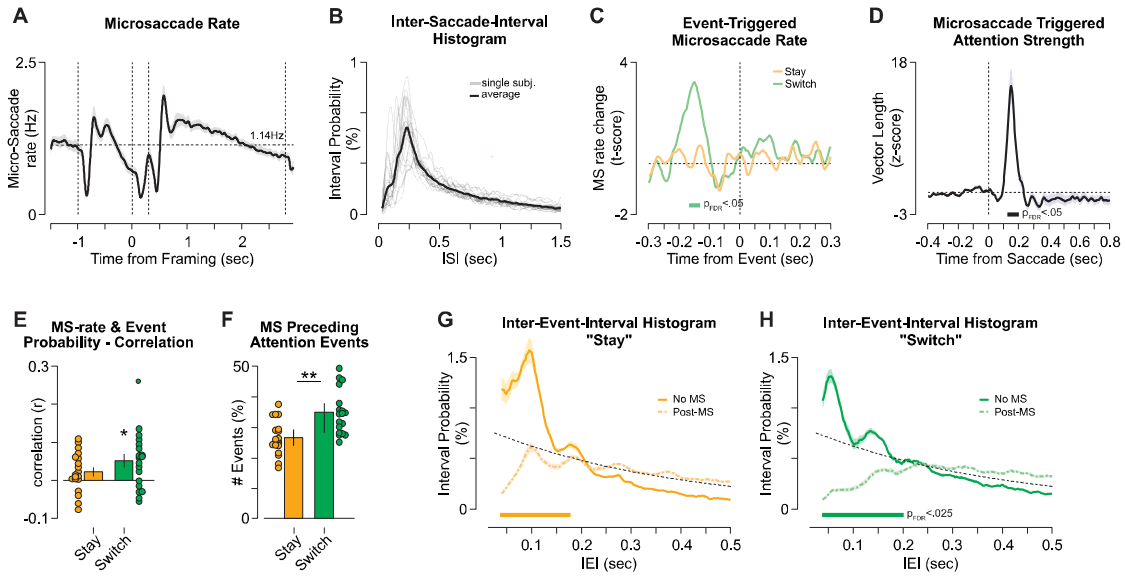

Figure 7. Attentional- and Microsaccade relations and dissociations.

(A) Average microsaccade (MS) rate during task execution. The thick line indicates the average over subjects and the shaded area the SEM. Vertical dashed lines indicate the stimulus onset, framing cue onset and offset as well as the stimulus offset (from left to right). The horizontal dashed line indicates the average MS rate over subjects, trials and the stimulus on period (1.14 Hz).

(B) Inter-saccade-interval histograms for micro-saccades. Thick and thin lines display the group-average and single-subject ISI histograms, respectively.

(C) Microsaccade rates pre- and post-attentional saccades, i.e. events, tested against shuffled events (t-test). Peri-event MS-rates around switch and stay events are depicted in green and orange. The thick colored bar denotes statistical significance ($p_{FDR} < 0.05$).

(D) Attention strength around microsaccade onset. The data is z-scored based on the 0.4 seconds prior to MS. The black line indicates the average over subjects and the shaded area the SEM. The thick bar denotes statistical significance from zero ($p_{FDR} < 0.05$).

(E) The correlation of the attentional event probability (Figure S9) with the trial-averaged MS rate (A) for each subject. The bars and vertical lines display the average and SEM over subjects, respectively. The colored dots represent the single subject Pearson correlation coefficients. The dots and bars are color-coded as in (C). Asterisk denotes significant correlations ($|r| > 0$, $p < 0.02$).

(F) Proportion of attentional events that were preceded by micro-saccades (dashed line) or another attention event (solid line) separately for refocus and switch events. Bars and vertical black lines display the mean and 25%-75% range. Asterisk denotes significant difference between switch and stay ($p < 0.001$).

(G-H) I Inter-event-interval histograms for refocus (F) and switch (H) attentional events split into events with (dashed) and without a microsaccade (solid line) after the previous event. Color-coded as above. The thick colored bar denotes statistical significance (No MS > post-MS; $p_{FDR} < 0.025$).

However, microsaccades did not show an effect on the rhythmicity of attentional events (Figure 7G,H). We calculated what effect a microsaccade occurring between two attentional events would have on the respective interval length. We found that microsaccades on average decrease the probability for short-latency intervals up to 0.2 s both for refocusing and switching attention (Figure 7G,H). A microsaccade thus appears to delay the upcoming attentional event. However, irrespective of microsaccades the underlying rhythmicity of event-intervals persisted. We detected rhythmicity, i.e. first-to-second peak latency (see Methods), for post-saccadic events in 15 out of 20 subjects for both event types with no detectable change in oscillation frequency ($t_{stay} < 1.8$, $p_{stay} > 0.1$; $t_{switch} < 1.1$, $p_{switch} > 0.3$).

In conclusion, microssacades had a marked effect on allocating attention between decision alternatives. However, microsaccades themselves cannot explain the dynamic aspects of attention allocation. Thus, our control analyses reported in this section indicate that the covert attentional saccades we focused on in this study cannot readily be inferred by monitoring eye movement patterns.

Discussion

Here, we show for the first time that rhythmic attentional sampling is a fundamental neurophysiological mechanism that helps to orchestrate attention and information sampling during challenging decisions. We identified that the strength of attention, i.e. attentional gain, was modulated at a frequency of 11 Hz during task processing. Hereby, peaks of the attention oscillation displayed increased processing of the attended decision alternative. On the other hand, during attention oscillation troughs we observed a strong tendency to reorient covert attention between decision alternatives.

Our findings thus provide a novel window into the neural basis of decision-making, which integrates recent insights into the rhythmic dynamics of covert attention with decision-relevant information sampling. While a decision maker is confronted with the complex task of sampling as much information as possible about each decision alternative and at the same the need to compare different options this conflict is resolved through rhythmicity[14,26]. By oscillating the attention strength, a feature potentially established through cortico-thalamic connections[30,58–60], reorienting and focusing modes of attention can be temporally multiplexed within each oscillatory cycle. Thus, focused information sampling can alternate with spatial re-allocation of the attentional spotlight without competing for the same cognitive resources. We consistently identified this mechanism on the single-subject level. In the following we will discuss how these different aspects of attention might further interact with the decision-making process and highlight three key findings.

One key finding is that information is sampled optimally over brief periods of time as a result of rhythmic attentional gain. At times of strong attentiveness participants were

more engaged[36–40] with the task (Figure S6) and more likely to increase processing of the attended decision alternative (Figure 5). Consequently, decision formation processes on the neuronal level might weigh incoming evidence in a similarly time dependent manner[61]. Along these lines we found that stronger attentional rhythmicity around 11 Hz might benefit the decision formation (Figure 4). Attention is not static[14,16,26], thus the effect of attention on information sampling likely is dynamic as well. Integrating covert attention as a time-varying variable both in locus as well as strength into existing models[1,5] of evidence accumulation might thus improve our understanding of dynamic decision making as well as the suboptimalities characterizing behavior in complex, multi-attribute contexts[8,62].

A second key finding is that reorienting attention between alternatives leads to marked changes in neuronal processing. We can observe these changes as a transient 'reset' of activity during attention switches. The reset consists of two components. First, due to the anti-phasic relationship to the ongoing attention oscillation, neuronal activity prior to events dissociates between switching and refocusing (Figure 5). Second, the dominant frequency of the attention oscillation is increased prior to reorienting (Figure 6). When attention is shifted from one option to another the predominant fluctuation frequency is restarted and aligned to neuronal activity compatible with refocus events. This alignment of activity, or reset, speaks for a transient interaction between the two modus operandi of attention and their related neural substrates (compare Figure S7 & S10). The reset might indicate readiness of the system to change[29] or be beneficial to internally transmit the allocation of attention to other processing stages[25,26,63]. In the context of decision formation a reset might signal a change in weighting evidence, i.e. drift rate, increasing weighting from attended and decreasing from unattended options (compare [63,64]). Similarly, a reorienting-related reset might indicate ongoing competition between the

previously and now attended option (compare [41]). However, further research is needed to better understand the impact switch-related resets have during decision making.

The third key finding is that looking at a decision alternative is not equivalent to attending and sampling information about it. Overt oculomotor responses, i.e. (micro-)saccades, can guide attention and neuronal processing[11,12,55,56] by also triggering an attentional saccade. We could show that fixational eye movements and microsaccades had a marked effect on reorienting attention between options (Figure 7). Microsaccades yielded a brief post-saccadic suppression of attentional event probability followed by a strengthening of the visual representation of the focused option around 0.15 – 0.2 s after a saccade. However, reciprocally not every covert reorienting leads to an overt response[9,10,50,63]. Microsaccades themselves did not display rhythmicity, inter-saccadic-intervals peaked later than attentional event intervals and microsaccades displayed a systematic relationship to switching but not refocusing attention. Lastly, the rhythmicity of attentional saccades was not affected by microsaccades. Our results thus show that covert and overt attention allocation are well dissociable. Where one is fixating and what is intrinsically being processed are thus not interchangeable units of attention and neural processing. Recent experimental and modeling literature focused on overt fixations and whether or not they can predict choice[2,3,5] and intrinsic value representations[1,6,7]. However, intrinsic processing and covert attention have been missing from the discussion so far and we offer a methodological framework to directly compare and dissociate overt from covert attention contributions to decision making.

Our approach differs from previous psychophysical and neurophysiological studies of rhythmic perception (or attention) by directly estimating the dynamics of the focus (i.e., strength and direction) of covert attention from neural data. Previous studies have either

quantified temporal fluctuations of behavioral performance[18,24,26–28,65] and/or of cortical population activity[15,17,18,20,23,24,27,30,31,65], without assessing the information content of the latter. By contrast, we here constructed content-specific decoders from patterns of cortical population activity (trained on independent localizer data) that enabled us to directly track the attentional focus, as it was expressed in selective patterns of cortical dynamics unfolding during the main decision-making task. Importantly, we could define dynamics in an unsupervised fashion and without assumptions on rhythmicity or temporal structure. Further, our multi-alternative choice task parallels features of top-down visual search protocols[27,31,32,66]: The initial framing decoupled the (bottom-up) stimulus intensity from the (top-down) task-relevance of the choice options. We can thus conclude that our findings and particularly the dominant attention oscillation frequency at 11 Hz were not purely driven by bottom-up sensory cortical responses (compare also Figure S2 & S3). Overall, our approach enabled us to make several new observations – first and foremost, that this highly specific neural measure of covert attention fluctuated rhythmically during information sampling in protracted decisions.

In conclusion, our findings highlight rhythmic attention as a general neurophysiological mechanism to resolve conflicts between neuronal processing stages in visual search, target detection, perception and, for the first time, decision-making. Here, the focused sampling of information and the re-allocation of attention between decision alternatives are multiplexed within an oscillatory cycle of about 0.1 seconds. In other words, when you want to choose between two desserts you might process one option intensely for about 0.05 seconds before you switch your attention to another delicacy during the next 0.05 seconds until you have made your choice. This type of choice-related covert attention is also distinct from overt oculomotor markers and grants a novel window into tracking the focus of attention online. Given our results the influence of attention and

thus stimulus processing on the formation of a decision needs to be reconsidered. Ultimately, we propose that sequential sampling models of decision-making will benefit from incorporating the momentary focus of attention into choice predictions.

Author Contributions

All authors contributed to the conceptualization and experimental protocol. M.S., Y.C. & M.T.M. collected the data. M.S. & Y.C. did the formal data analysis and M.S. visualized the results. M.S., T.H.D. & K.T. wrote the initial draft, all authors contributed to editing the manuscript.

Methods

Subjects and experimental procedure

20 subjects (9 female, age_{mean} = 28.05 years ± age_{STD} 4.6 years) participated in a three-alternative decision-making task with variable task framing. The experiment was approved by the ethics committee of the Hamburg Medical Association and conducted in accordance with the Declaration of Helsinki. All subjects gave their written informed consent and received monetary compensation for their participation.

Decision-making task. During central fixation three Gabor patches (spatial frequency) of varying contrast levels and orientations appeared on screen. The stimuli were presented peripherally (2.2^o eccentricity, 1.6^o stimulus diameter) at the top and 120° left and right of it. The three stimuli were drawn without replacement from a set of five linearly spaced contrast levels (10 possible combinations). We derived the distance between neighboring contrast levels via a staircase procedure individually within each subject. The patch orientations were drawn from a set of three equally distant orientations with either all three being identical or different. After 1 second into the stimulus presentation a central framing cue (0.3 sec.) indicated the target contrast, either the highest ("Hig") or lowest ("Low"). We randomized the task framing between trials. After the framing cue offset the central fixation cross re-appeared and initiated a fixed decision phase (2.5 sec.). The three Gabor stimuli were visible and unaltered all throughout the 3.8 seconds stimulus period. After the stimuli turned off the fixation cross rotated 45° and cued the response. Subjects had 2 seconds to indicate their decision with a left thumb, right thumb or foot button press for the left, right or top option, respectively. We randomized the foot (left or right) between subjects. To visually guide the subjects we tilted the entire stimulus array 6° clockwise or counter-clockwise when subjects were using their right or left foot, respectively. Task framing, contrast levels, Gabor orientation and stimulus

locations were fully randomized, yielding a total of 1080 unique trials. The trials were blocked into random sets of 120 trials and each subjects concluded two full randomization runs (18 blocks).

Sensory localizer. Prior to each block of the decision-making task the subjects concluded a sensory localizer block. Each block consisted of 90 consecutive 0.35-second presentations of single Gabor stimuli at full contrast with 0.5 seconds inter-trial intervals. Each stimulus was presented with the same size and eccentricity as during the decision-making task. We instructed the subjects to ignore the peripheral stimuli and fixate at the center. The subjects' task was to detect a flickering of the central fixation cross that could occur randomly at each stimulus, in total 9 times per block, and indicate the detection with a finger button press. We excluded trials with flicker presentation from further analyses. In each block we fully randomized the orientation and the position over the three locations. Each unique stimulus combination was repeated ten times paired once with a central fixation flickering.

Functional data acquisition and preprocessing

Data acquisition. During the experiment the participants were sitting upright in a whole-head magnetoencephalography scanner (MEG; 275 axial gradiometer sensors, CTF Systems Inc.) in a magnetically shielded room. The data was acquired at a sampling rate of 1200 Hz. Each participant's head position was tracked online using three head localization coils (nasion, left/right preauricular points). Additionally, we recorded a 2-channel bipolar electro-oculogram (horizontal and vertical EOG) and a single channel bipolar electro-cardiogram (ECG) to control for cardiovascular and ocular signal artifacts. Eye-movements and pupil diameter were tracked with an MEG-compatible Eyelink 1000 system (SR Research). We further collected T1-weighted structural magnetic resonance images (MRI; sagittal MP-RAGE) to reconstruct individualized high-resolution head models.

Preprocessing. We band-pass filtered the continuous MEG data segments between 0.2 and 200 Hz (4th order Butterworth filter) and down-sampled it to 400 Hz. Next, we filtered the line noise with a notch filter at 50 Hz and its first 6 harmonics (1 Hz stop-band filter width). We implemented a two-stage procedure for artifact rejection[67,68]: First, we inspected all data segments for technical- (i.e. SQUID-jumps, passing cars), muscle- and eye-blink artifacts and excluded corresponding time intervals from further analyses. Second, we filtered the data into two distinct frequency ranges, a low- from 0.2 to 30 Hz and a high-range from 30 to 200 Hz, with a 4th order Butterworth filter. We computed independent component analyses[69] (ICA) on both frequency ranges separately. This approach takes advantage of the intrinsic properties of different artifact types. On the one hand, eye-blinks eye-movements, passing cars and cardiovascular artifacts display predominantly low-frequency features. On the other hand, muscle activity shows the strongest effects in higher frequencies. We visually inspected the independent components, rejected artifact components based on their topology, power-spectra and time-courses[68,70] and subsequently recombined both frequency bands.

Spectral analysis and source reconstruction

Spectral analysis. We estimated time-frequency representations of the time-domain MEG signals using Morlet's wavelets[71]. We set the wavelet bandwidth at 0.5 octaves ($f/\sigma t = 5.83$, kernel width at σt) and derived complex spectral estimates for frequencies between 2 to 90.5 Hz in quarter octave steps (2^1 to $2^{6.5}$ Hz).

Source projection. Based on each subjects individual structural MRI we generated single-shell boundary-element method models[72,73] (BEM) and computed the physical forward model (leadfields) for 457 equally spaced cortical sources[74,75] (~1.2 cm distance, at 0.7 cm depth below pial surface). Sensor locations, source and leadfield positions were co-registered to the common MNI-space using the position of the three head-localization coils. We applied dynamic imaging of coherent sources[76,77] (DICS) linear

beamforming to estimate source-level neuronal activity. DICS is a spatial filtering approach that reconstructs activity at the source of interest with unit gain while at the same time maximally suppressing signal contributions from other sources.

Encoding the focus of covert attention

To reconstruct the focus of covert attention during free information sampling of multiple stimuli we implemented an inverted encoding model[44,45]. The modeled activity hereby displays momentary changes of the visual representations of the presented stimuli (compare also Figure 2). The model assumes that the sensor-level MEG activity can be described as a weighted sum of distinct abstract neuronal populations, i.e. information channels, with individual tuning properties to the angular positions plus noise *N*[44,45].

$$MEG_{Loc} = WC_{Loc} + N$$

We trained the encoding model on the functional localizer task MEG_{Loc}. C_{Loc} was a design matrix describing a set of basis functions, i.e. the tuning curves, for each information channel (see Figure 2A) and *W* described the weight matrix specifying the relationship between the information channels and the neuronal data. Each information channel was modelled as a half-wave rectified sinusoidal filter *f* with a fifth power exponent ($\alpha = 5$). We derived the basis functions *f* for the design matrix as

$$f = |cos^{\alpha}[0.5(\theta - \mu)\pi/180]|$$

Here, θ is a continuous variable indicating the angular position relative to central fixation, and μ the preferred angle of each filter (θ and μ are in degrees, with 0° pointing upward along the vertical midline and angular value increasing counter-clockwise e.g., 90° pointing leftward). α was the power exponent set to 5. The target stimuli were set to μ = 0°, 120° and 240° for top, left and right, respectively. During the functional localizer task only one stimulus out of the full set has been visible on screen. Hence, we trained the model during the localizer, as both MEG_{Loc} and C_{Loc} were known variables. We estimated the weight matrix *W* (sensors x information channels) as follows

$$w_k = MEG_{Loc} c_{Loc,k}^T (c_{Loc,k} c_{Loc,k}^T)^{-1}$$

Where w_k denotes the weights of the *kth* information channel $c_{Loc,k}$, i.e. a single tuning curve. As neighboring MEG channels are not independent estimates of neuronal activity due to volume conduction we further included multivariate noise normalization to improve the pattern reliability[78]. Thus, we transformed each w_k into the pre-whitened weighting vector g_k

$$g_k = \frac{\mathrm{E}_k^{-1} w_k}{w_k^T \mathrm{E}_k^{-1} w_k}$$

Where *E* is the noise covariance matrix for channel *k* using the channels noise term as $\varepsilon_k = MEG_{Loc} - w_k c_{Loc,k}$. *E* was regularized by shrinking it towards the diagonal matrix, using the optimal shrinkage factor, i.e., minimizing the expected squared loss of the resultant covariance estimator[79]. With the optimized weight-matrix *G* we can estimate the latent visual representation of the stimuli during the multi-alternative decision-making task (see Figure 2B). Therefore, we invert the encoding model

$$C_{MDM} = G^T MEG_{MDM}$$

C_{MDM} comprises the estimated response as the representational activity distribution over angular positions for each time point during the task. The strength of the representation indexes the covert visual attention towards each target on screen.

Lastly, we reconstructed the momentary spatial focus as the vector sum over the three estimated stimulus activities. The vector orientations were set to 0°, 120° and 240° for the top, left and right stimulus, respectively and the corresponding length at each orientation from the channel response C_{MDM}. This reconstructed attentional vector visualizes two main characteristics of spatial attention, namely the overall attention paid at each time point and from which target information is sampled. We considered the attentional vector length as a proxy of overall attention and the maximum of the angular similarity to the displayed options as the most likely target of covert spatial attention.

We trained the model for different time points during the localizer task with respect to stimulus onset. To achieve the best decoding performance we selected the optimal training epoch using cross-validation (leave-one-block-out, 18 blocks per subject) within the sensory localizer task. We found decoding strength to peak between 140 to 170 msec post stimulus onset (Figure S1) and averaged the MEG signal over this period to construct the decoding model for the application on the MEG_{MDM} data.

Spectral analysis of attention strength

We computed time-frequency resolved estimates of the attentional vector length to assess the spectral dynamics of attention strength. We band-pass filtered (4th order Butterworth filter) the trialed vector length (f_{sample} = 400 Hz, from -1.5 seconds relative to stimulus onset to 2 seconds after stimulus offset) to center frequencies between 2.8 Hz to 90.5 Hz in quarter octave steps ($2^{1.5}$ to $2^{6.5}$). The pass-band covered the center frequency plus/minus half an octave, e.g. for $2^{1.5}$ Hz center frequency we filtered the data between 2^1 and 2^2 Hz. We estimated the frequency dependent attention strength as the absolute value of the complex Hilbert transform from the time-domain vector length signal. To exclude edge artifacts we cut two cycles of the center frequency from the beginning and end of each trial. We visualized the data between -1.5 to +3 seconds relative to the framing cue onset. We applied the same procedure for the reconstructed stimulus activities at each location (compare Figure S2 & S3).

For the analysis of attention strength fluctuations as a function of correct versus error trials we stratified the included trials. Hereby, we matched the numbers of trials included from each of the 10 possible contrast combinations per framing condition. For all subjects we identified more correct choices than error choices in all stimulus combinations. We thus randomly subsampled one hundred times from all correct trials according to the stratification assumptions and averaged the spectral amplitude and the vector length over repetitions before comparing against error trials (see Figure 4).

Defining attentional events

We estimated the momentary focus of spatial attention via the angular similarity of the attentional vector to the three stimuli on screen. At each point in time the attentional vector can display the focus to be close to one or in between targets. To investigate the dynamics of information sampling, i.e. when one option is strongly focused, we thresholded the maximum angular similarity at the subject-specific 90th percentile over the entire dataset. However, as the vector orients in circular space and even under completely random conditions will point towards one of the three stimuli at times we added a second threshold on the vector length (90th percentile within a trial). Thus, we recorded attentional events when both thresholds were crossed at the same time. In other words, we traced points in time when subjects were both attentive and locked on one stimulus. We recorded the first time point of passing both thresholds as an event onset and excluded events occurring within 0.025 sec after the previous onset.

Event dynamics. To assess the dynamics of these attentional saccades we investigated the intervals between subsequent events. Here, we recorded the time from event *e* onset to the onset of event *e+1* within a trial and generated inter-event-interval (IEI) histograms over all events and trials within a subject. We excluded intervals reaching over trials. The histograms were computed over a median of 17,696 events per subject (range 12,377 to 28,909; compare Figure S4). We further generated Null-models for inference statistical testing using randomization. Hereby, we randomized the trial each event was belonging to while keeping its position within the trial. In other words, when we detected for example 10 events at time point *t* scattered over 2160 trials, we randomly reassigned trial identities to these events (without replacement) and proceeded in the same way with time point *t+1*. We computed the IEI histogram after every randomization run. With this approach we can randomize event relationships

without tempering with the task-dependent dynamics. We repeated the randomization step 1000 times for each subject.

Event sequences. We further tracked first order event sequences. An event can occur either at the same stimulus location as the one before or a different location, i.e. a subject either refocuses or reorients their attention. We generated IEI histograms and the randomization for both event types separately and statistically tested interval probabilities against the mean of the randomized Null-models (one-sided paired t-test). Hereby, we obtained t-scores for each interval from 0.025 to 0.5 seconds (at f_{sample} = 400 Hz) for both refocus and reorient.

Interval-probability fluctuations. If we assume that attention is rhythmic then attentional events would occur probabilistically at preferential phases within an underlying oscillation and we would expect to observe distinct peaks in the IEI histograms: The first peak would display the preferential phase within the first oscillatory cycle, the second peak the second cycle, etc. Thus, we can estimate the prevalent attentional fluctuation frequency as the inverse of the latency between peaks. Therefore, we subtracted the subject-specific expected IEI histogram (Null-model) from the observed histogram. All non-significant values were set to zero according to random-effect statistics based on randomization (one-sided paired t-test against zero, $p < 0.01$; see also above). We smoothed the resulting truncated histograms twice with a 0.01 sec boxcar kernel, padding the edges to the first and last histogram value. Finally, we extracted the local maxima of the truncated and smoothed histograms. Overall, we identified one significant peak in 17 and 18 subjects and at least two peaks in 16 and 17 subjects for the refocus- and reorient-IEI histograms, respectively. For further analyses we defined the cycle length of the attention rhythm as the latency from the first to the second peak.

Threshold assessment. We further controlled for effects of the applied threshold through a systematic assessment for a wide range of threshold choices. In theory, if the

thresholds are too liberal the analysis will include several random events converging the IEI histogram to an exponential decay. If the threshold is too high there won't be enough events to have sufficient statistical power for the full IEI distribution. We varied the applied thresholds between the 50% and 95% percentile in 5% steps as well as for the 97.5% and 99% percentile separately for the maximum angular similarity and the vector length (Figure S11). This approach yielded a total of 144 (12 x 12) threshold combinations. We replicated our main findings (individual peaks in the IEI histogram) for a variety of threshold choices between the 80% and 95% percentile (Figure S11A-B). Importantly, the timing of histogram peaks appeared to be stable over thresholds. Further, we quantified the deviation of the histogram from an exponential decay, i.e. randomly distributed events, through the variability of interval probabilities further referred to as modulation intensity. Hereby, we first log-transformed the interval probabilities and linearly detrended the resulting values. Next, we smoothed these distributions with a 0.025 second (10 samples) box-car kernel twice and defined local maxima. Finally, we computed the modulation intensity as the standard deviation of the detrended histogram between the first and second maximum (Figure S11C-D). We found the strongest median modulation intensity for the highest vector length thresholds at over 95% with variably applicable thresholds for the MAS. Further increasing both thresholds beyond the 95% percentile yielded inconclusive modulation in several subjects due to a lack of identifiable events (Figure S11E-F). We thus conclude that our main findings are threshold invariant within a sensible range between the 80% to 97.5% percentile with an optimal range approximately between the 90% and 95% percentile for both parameters. At the 90% percentile threshold for both measures, i.e. the applied threshold during the main text, thus granted both reasonably reliable modulation intensity and further a sufficient number of attentional events to increase statistical power for event-triggered analyses (Figure S11G-H). Finally, the optimal threshold

parameters depend on the research question, the number and the length of the trials. It is thus pivotal to control these parameters for each new analysis. However, we must stress that optimizing the parameters does not evoke rhythmicity or temporal structure but can only reveal existing structure.

Peri-event fluctuations of attention

To compare the dynamics leading up to attentional events we investigated the event-triggered fluctuations of attention from 0.2 sec before to 0.2 sec after each event. Here, we averaged the attention strength, i.e. attention vector length, and the attention focus, i.e. maximum angular similarity, over all events within each subject and z-scored the traces according to the distribution between -0.2 to -0.03 sec (pre-event period) and 0.03 to 0.2 sec (post-event period) before averaging over subjects. We excluded the peri-event period (± 0.03 sec.) from normalization as the event itself, by definition the highest values, would skew the distribution. For further visualization we de-trended and smoothed the event-triggered traces with a 0.025 sec boxcar kernel separately for the pre- and post-event period. Further, we used the de-trended and smoothed traces to define prominent peri-event fluctuation frequencies via the inverse of the average peak-to-peak latencies.

Pupillometry and microsaccade analysis

We tracked the eye-gaze and pupil size of the right eye at 1000 Hz sampling rate with an EyeLink 1000 Long Range Mount (SR Research, Osgoode, Canada). We calibrated the eye-tracker at the start of each block. The average spatial resolution was between 15 – 30 min arc. We down-sampled the sampling to 400 Hz compatible to the MEG data.

Defining pupil responses. We detected blinks according to the MEG preprocessing pipeline and saccades using the algorithm provided by SR Research with default settings. Within each subject we normalized the average pupil size between the 5% and

95% percentile. We derived the change in pupil diameter as the temporal derivative of the pupil size by subtracting adjacent frames.

Microsaccade detection. We defined microsaccades as brief events of high gaze velocity. We computed gaze velocity as the Euclidean distance in fixation position, i.e. between x- and y-coordinates, over neighboring frames. We further smoothed the velocity with a 0.02 s box-car kernel and z-scored within each trial. Then we defined samples exceeding $z > 3$ as microsaccades. Furthermore, to avoid counting the same event multiple times we imposed a minimum delay of 0.025 s between microsaccades. The microsaccade rate was generated as the saccade probability over trials at each sample multiplied by the sampling rate (400 Hz).

Relating micro- and attentional saccades. We assessed the attentional event-triggered microsaccade rate in time-windows between -0.3 to 0.3 s from attention event onset and averaged over events separately for refocusing and reorienting. We compared the average microsaccade rate within these windows against trial-shuffled attention-event definitions (see also above), i.e. the change in microssacade rate. We further analyzed the microsaccade triggered attention strength, i.e. vector length, in a time-window between -0.4 to 0.8 s from microsaccade onset. Finally, we investigated the effect of microsaccades on the rhythmicity of attentional events by re-computing the inter-event-interval histograms separately for intervals containing or not containing a microsaccade.

Neural correlates of covert attentional saccades

We computed the neuronal signal strength, i.e. the amplitude envelope, over the entire cortex to assess the relationship to attentional events (see also Spectral analysis and source reconstruction). According to our results (Figure 3E & 5C) we focused the analysis on the alpha (11 Hz), beta (22 Hz) and gamma (40 Hz) frequency range. According to the literature we further included the theta frequency range (4 Hz)[14,26,27]. Within each subject and source we correlated the frequency-specific signal amplitude

envelope with the event probability throughout the stimulus on period. For each event type as well as the difference between them we tested the correlation against zero over subjects (two-sided t-test).

Correlation with attention strength. We further computed the correlation between the neural signal envelopes and the corresponding band-limited attentional fluctuations.

Event-triggered neural signals. To assess the relationship between event-triggered attention- and neural modulations we averaged over signal amplitudes for switch and refocusing events separately in each cortical source for a time window of ± 0.3 sec relative to event onset. We z-scored the neuronal activity within each window prior to averaging over events and subjects. For visualization purposes we grouped a subset of cortical sources into four regions-of-interest[14,19,26] approximating: early visual areas including V1, medial parietal cortex, medial prefrontal cortex (mPFC) and the dorsolateral prefrontal cortex (dlPFC) including the frontal eye field (FEF)[74]. The average ROI activity was statistically compared between event types using a two-sided paired t-test.

References

1. Krajbich, I. (2019). Accounting for attention in sequential sampling models of decision making. Curr. Opin. Psychol. *29*, 6–11. 10.1016/j.copsyc.2018.10.008.
2. Orquin, J.L., and Mueller Loose, S. (2013). Attention and choice: A review on eye movements in decision making. Acta Psychol. (Amst.) *144*, 190–206. 10.1016/j.actpsy.2013.06.003.
3. Krajbich, I., and Rangel, A. (2011). Multialternative drift-diffusion model predicts the relationship between visual fixations and choice in value-based decisions. Proc. Natl. Acad. Sci. *108*, 13852–13857. 10.1073/pnas.1101328108.
4. Busemeyer, J.R., and Townsend, J.T. (1993). Decision field theory: a dynamic-cognitive approach to decision making in an uncertain environment. Psychol. Rev. *100*, 432.
5. Krajbich, I., Armel, C., and Rangel, A. (2010). Visual fixations and the computation and comparison of value in simple choice. Nat. Neurosci. *13*, 1292–1298.
6. Mormann, M., and Russo, J.E. (2021). Does Attention Increase the Value of Choice Alternatives? Trends Cogn. Sci. *25*, 305–315. 10.1016/j.tics.2021.01.004.
7. Smith, S.M., and Krajbich, I. (2019). Gaze Amplifies Value in Decision Making. Psychol. Sci. *30*, 116–128. 10.1177/0956797618810521.
8. Noguchi, T., and Stewart, N. (2014). In the attraction, compromise, and similarity effects, alternatives are repeatedly compared in pairs on single dimensions. Cognition *132*, 44–56.
9. Liu, B., Nobre, A.C., and van Ede, F. (2022). Functional but not obligatory link between microsaccades and neural modulation by covert spatial attention. Nat. Commun. *13*, 3503.
10. Gaillard, C., Ben Hadj Hassen, S., Di Bello, F., Bihan-Poudec, Y., VanRullen, R., and Ben Hamed, S. (2020). Prefrontal attentional saccades explore space rhythmically. Nat. Commun. *11*, 925. 10.1038/s41467-020-14649-7.
11. Moore, T., and Armstrong, K.M. (2003). Selective gating of visual signals by microstimulation of frontal cortex. Nature *421*, 370–373. 10.1038/nature01341.
12. Krauzlis, R.J., Lovejoy, L.P., and Zénon, A. (2013). Superior Colliculus and Visual Spatial Attention. Annu. Rev. Neurosci. *36*, 165–182. 10.1146/annurev-neuro-062012-170249.
13. Posner, M.I. (2016). Orienting of attention: Then and now. Q. J. Exp. Psychol. 2006 *69*, 1864–1875. 10.1080/17470218.2014.937446.
14. Fiebelkorn, I.C., and Kastner, S. (2019). A Rhythmic Theory of Attention. Trends Cogn. Sci. *23*, 87–101. 10.1016/j.tics.2018.11.009.
15. Fiebelkorn, I.C., Saalmann, Y.B., and Kastner, S. (2013). Rhythmic Sampling within and between Objects despite Sustained Attention at a Cued Location. Curr. Biol. *23*, 2553–2558. 10.1016/j.cub.2013.10.063.
16. VanRullen, R. (2016). Perceptual Cycles. Trends Cogn. Sci. *20*, 723–735. 10.1016/j.tics.2016.07.006.
17. Busch, N.A., and VanRullen, R. (2010). Spontaneous EEG oscillations reveal periodic sampling of visual attention. Proc. Natl. Acad. Sci. *107*, 16048–16053.

10.1073/pnas.1004801107.
18. Landau, A.N., and Fries, P. (2012). Attention samples stimuli rhythmically. Curr. Biol. CB *22*, 1000–1004. 10.1016/j.cub.2012.03.054.
19. Fiebelkorn, I.C., and Kastner, S. (2020). Functional specialization in the attention network. Annu. Rev. Psychol. *71*, 221–249.
20. VanRullen, R., Carlson, T., and Cavanagh, P. (2007). The blinking spotlight of attention. Proc. Natl. Acad. Sci. *104*, 19204–19209.
21. Fiebelkorn, I.C. (2022). Detecting attention-related rhythms: When is behavior not enough?(Commentary on van der Werf et al. 2021). Eur. J. Neurosci. *55*, 3117–3120.
22. Mo, C., Lu, J., Wu, B., Jia, J., Luo, H., and Fang, F. (2019). Competing rhythmic neural representations of orientations during concurrent attention to multiple orientation features. Nat. Commun. *10*, 5264.
23. Fiebelkorn, I.C., Pinsk, M.A., and Kastner, S. (2018). A Dynamic Interplay within the Frontoparietal Network Underlies Rhythmic Spatial Attention. Neuron *99*, 842-853.e8. 10.1016/j.neuron.2018.07.038.
24. Helfrich, R.F., Fiebelkorn, I.C., Szczepanski, S.M., Lin, J.J., Parvizi, J., Knight, R.T., and Kastner, S. (2018). Neural Mechanisms of Sustained Attention Are Rhythmic. Neuron *99*, 854-865.e5. 10.1016/j.neuron.2018.07.032.
25. Landau, A.N., Schreyer, H.M., van Pelt, S., and Fries, P. (2015). Distributed Attention Is Implemented through Theta-Rhythmic Gamma Modulation. Curr. Biol. CB *25*, 2332–2337. 10.1016/j.cub.2015.07.048.
26. Fries, P. (2023). Rhythmic attentional scanning. Neuron *111*, 954–970. 10.1016/j.neuron.2023.02.015.
27. Senoussi, M., Moreland, J.C., Busch, N.A., and Dugué, L. (2019). Attention explores space periodically at the theta frequency. J. Vis. *19*, 22–22.
28. Abdalaziz, M., Redding, Z.V., and Fiebelkorn, I.C. (2023). Rhythmic temporal coordination of neural activity prevents representational conflict during working memory. Curr. Biol. *33*, 1855–1863.
29. Buschman, T.J., and Kastner, S. (2015). From behavior to neural dynamics: an integrated theory of attention. Neuron *88*, 127–144.
30. Fiebelkorn, I.C., Pinsk, M.A., and Kastner, S. (2019). The mediodorsal pulvinar coordinates the macaque fronto-parietal network during rhythmic spatial attention. Nat. Commun. *10*, 1–15.
31. Kienitz, R., Schmid, M.C., and Dugué, L. (2022). Rhythmic sampling revisited: experimental paradigms and neural mechanisms. Eur. J. Neurosci. *55*, 3010–3024.
32. Dugué, L., Roberts, M., and Carrasco, M. (2016). Attention reorients periodically. Curr. Biol. *26*, 1595–1601.
33. Bellet, J., Chen, C.-Y., and Hafed, Z.M. (2017). Sequential hemifield gating of α- and β-behavioral performance oscillations after microsaccades. J. Neurophysiol. *118*, 2789–2805.
34. Pfeffer, T., Keitel, C., Kluger, D.S., Keitel, A., Russmann, A., Thut, G., Donner, T.H., and Gross, J. (2022). Coupling of pupil-and neuronal population dynamics reveals diverse influences of arousal on cortical processing. elife *11*, e71890.
35. Radetz, A., and Siegel, M. (2022). Spectral fingerprints of cortical neuromodulation. J. Neurosci. *42*, 3836–3846.

36. Wainstein, G., Whyte, C., Martens, K.E., Müller, E., Munn, B., Medel, V., Anderson, B., Stöttinger, E., Danckert, J., and Shine, J. (2022). Noradrenergic modulation of whole brain dynamics mediates perceptual switches.
37. Reimer, J., McGinley, M.J., Liu, Y., Rodenkirch, C., Wang, Q., McCormick, D.A., and Tolias, A.S. (2016). Pupil fluctuations track rapid changes in adrenergic and cholinergic activity in cortex. Nat. Commun. *7*, 13289.
38. Preuschoff, K., 't Hart, B.M., and Einhäuser, W. (2011). Pupil dilation signals surprise: Evidence for noradrenaline's role in decision making. Front. Neurosci. *5*, 115.
39. Jepma, M., and Nieuwenhuis, S. (2011). Pupil Diameter Predicts Changes in the Exploration–Exploitation Trade-off: Evidence for the Adaptive Gain Theory. J. Cogn. Neurosci. *23*, 1587–1596. 10.1162/jocn.2010.21548.
40. Dahl, M.J., Mather, M., and Werkle-Bergner, M. (2022). Noradrenergic modulation of rhythmic neural activity shapes selective attention. Trends Cogn. Sci. *26*, 38–52.
41. Odean, N.N., Sanayei, M., and Shadlen, M.N. (2022). Transient oscillations of neural firing rate associated with routing of evidence in a perceptual decision. Preprint at bioRxiv, 10.1101/2022.02.07.478903 10.1101/2022.02.07.478903.
42. Benedetto, A., Morrone, M.C., and Tomassini, A. (2020). The common rhythm of action and perception. J. Cogn. Neurosci. *32*, 187–200.
43. Schroeder, C.E., Wilson, D.A., Radman, T., Scharfman, H., and Lakatos, P. (2010). Dynamics of active sensing and perceptual selection. Curr. Opin. Neurobiol. *20*, 172–176.
44. Sprague, T.C., and Serences, J.T. (2013). Attention modulates spatial priority maps in the human occipital, parietal and frontal cortices. Nat. Neurosci. *16*, 1879–1887.
45. Brouwer, G.J., and Heeger, D.J. (2009). Decoding and reconstructing color from responses in human visual cortex. J. Neurosci. *29*, 13992–14003.
46. Aston-Jones, G., and Cohen, J.D. (2005). An integrative theory of locus coeruleus-norepinephrine function: adaptive gain and optimal performance. Annu Rev Neurosci *28*, 403–450.
47. Harris, K.D., and Thiele, A. (2011). Cortical state and attention. Nat. Rev. Neurosci. *12*, 509–523.
48. Lee, S.-H., and Dan, Y. (2012). Neuromodulation of brain states. neuron *76*, 209–222.
49. Donner, T.H., and Siegel, M. (2011). A framework for local cortical oscillation patterns. Trends Cogn. Sci. *15*, 191–199. 10.1016/j.tics.2011.03.007.
50. Buschman, T.J., and Miller, E.K. (2009). Serial, covert shifts of attention during visual search are reflected by the frontal eye fields and correlated with population oscillations. Neuron *63*, 386–396.
51. Gaillard, C., and Ben Hamed, S. (2022). The neural bases of spatial attention and perceptual rhythms. Eur. J. Neurosci. *55*, 3209–3223.
52. Corneil, B.D., and Munoz, D.P. (2014). Overt responses during covert orienting. Neuron *82*, 1230–1243.
53. Wang, C.-A., and Munoz, D.P. (2015). A circuit for pupil orienting responses: implications for cognitive modulation of pupil size. Curr. Opin. Neurobiol. *33*, 134–

140. 10.1016/j.conb.2015.03.018.
54. Wang, C.-A., and Munoz, D.P. (2021). Differentiating global luminance, arousal and cognitive signals on pupil size and microsaccades. Eur. J. Neurosci. *54*, 7560–7574. 10.1111/ejn.15508.
55. Hafed, Z.M., and Clark, J.J. (2002). Microsaccades as an overt measure of covert attention shifts. Vision Res. *42*, 2533–2545.
56. Hafed, Z.M., Lovejoy, L.P., and Krauzlis, R.J. (2011). Modulation of microsaccades in monkey during a covert visual attention task. J. Neurosci. *31*, 15219–15230.
57. Laubrock, J., Kliegl, R., Rolfs, M., and Engbert, R. (2010). When do microsaccades follow spatial attention? Atten. Percept. Psychophys. *72*, 683–694. 10.3758/APP.72.3.683.
58. Saalmann, Y.B., Pinsk, M.A., Wang, L., Li, X., and Kastner, S. (2012). The Pulvinar Regulates Information Transmission Between Cortical Areas Based on Attention Demands. Science *337*, 753–756. 10.1126/science.1223082.
59. Eradath, M.K., Pinsk, M.A., and Kastner, S. (2021). A causal role for the pulvinar in coordinating task-independent cortico–cortical interactions. J. Comp. Neurol. *529*, 3772–3784. 10.1002/cne.25193.
60. Griffiths, B.J., Zaehle, T., Repplinger, S., Schmitt, F.C., Voges, J., Hanslmayr, S., and Staudigl, T. (2022). Rhythmic interactions between the mediodorsal thalamus and prefrontal cortex precede human visual perception. Nat. Commun. *13*, 3736.
61. Wyart, V., De Gardelle, V., Scholl, J., and Summerfield, C. (2012). Rhythmic fluctuations in evidence accumulation during decision making in the human brain. Neuron *76*, 847–858.
62. Tsetsos, K., Moran, R., Moreland, J., Chater, N., Usher, M., and Summerfield, C. (2016). Economic irrationality is optimal during noisy decision making. Proc. Natl. Acad. Sci. *113*, 3102–3107. 10.1073/pnas.1519157113.
63. Stine, G.M., Trautmann, E.M., Jeurissen, D., and Shadlen, M.N. (2023). A neural mechanism for terminating decisions. Neuron.
64. Gold, J.I., and Shadlen, M.N. (2007). The neural basis of decision making. Annu. Rev. Neurosci. *30*, 535–574. 10.1146/annurev.neuro.29.051605.113038.
65. Raposo, I., Szczepanski, S.M., Haaland, K., Endestad, T., Solbakk, A.-K., Knight, R.T., and Helfrich, R.F. (2023). Periodic attention deficits after frontoparietal lesions provide causal evidence for rhythmic attentional sampling. Curr. Biol.
66. Dugué, L., Marque, P., and VanRullen, R. (2015). Theta oscillations modulate attentional search performance periodically. J. Cogn. Neurosci. *27*, 945–958.
67. Siems, M., Pape, A.-A., Hipp, J.F., and Siegel, M. (2016). Measuring the cortical correlation structure of spontaneous oscillatory activity with EEG and MEG. NeuroImage *129*, 345–355. 10.1016/j.neuroimage.2016.01.055.
68. Hipp, J.F., and Siegel, M. (2013). Dissociating neuronal gamma-band activity from cranial and ocular muscle activity in EEG. Front. Hum. Neurosci. *7*, 338. 10.3389/fnhum.2013.00338.
69. Hyvärinen, A., and Oja, E. (2000). Independent component analysis: algorithms and applications. Neural Netw. Off. J. Int. Neural Netw. Soc. *13*, 411–430.
70. Chaumon, M., Bishop, D.V.M., and Busch, N.A. (2015). A practical guide to the selection of independent components of the electroencephalogram for artifact

correction. J. Neurosci. Methods *250*, 47–63. 10.1016/j.jneumeth.2015.02.025.
71. Goupillaud, P., Grossmann, A., and Morlet, J. (1984). Cycle-octave and related transforms in seismic signal analysis. Geoexploration *23*, 85–102. 10.1016/0016-7142(84)90025-5.
72. Oostenveld, R., Fries, P., Maris, E., and Schoffelen, J.-M. (2010). FieldTrip: Open Source Software for Advanced Analysis of MEG, EEG, and Invasive Electrophysiological Data. Comput. Intell. Neurosci. *2011*, e156869. 10.1155/2011/156869.
73. Nolte, G. (2003). The magnetic lead field theorem in the quasi-static approximation and its use for magnetoencephalography forward calculation in realistic volume conductors. Phys. Med. Biol. *48*, 3637. 10.1088/0031-9155/48/22/002.
74. Hipp, J.F., and Siegel, M. (2015). BOLD fMRI Correlation Reflects Frequency-Specific Neuronal Correlation. Curr. Biol. CB *25*, 1368–1374. 10.1016/j.cub.2015.03.049.
75. Siems, M., and Siegel, M. (2020). Dissociated neuronal phase- and amplitude-coupling patterns in the human brain. NeuroImage, 116538. 10.1016/j.neuroimage.2020.116538.
76. Gross, J., Kujala, J., Hamalainen, M., Timmermann, L., Schnitzler, A., and Salmelin, R. (2001). Dynamic imaging of coherent sources: Studying neural interactions in the human brain. Proc. Natl. Acad. Sci. U. S. A. *98*, 694–699. 10.1073/pnas.98.2.694.
77. Van Veen, B.D., van Drongelen, W., Yuchtman, M., and Suzuki, A. (1997). Localization of brain electrical activity via linearly constrained minimum variance spatial filtering. IEEE Trans. Biomed. Eng. *44*, 867–880. 10.1109/10.623056.
78. Kok, P., Mostert, P., and De Lange, F.P. (2017). Prior expectations induce prestimulus sensory templates. Proc. Natl. Acad. Sci. *114*, 10473–10478.
79. Ledoit, O., and Wolf, M. (2004). A well-conditioned estimator for large-dimensional covariance matrices. J. Multivar. Anal. *88*, 365–411.